



CHORUS

This is the accepted manuscript made available via CHORUS. The article has been published as:

Effect of long- and short-range order on SiGe alloy thermal conductivity: Molecular dynamics simulation

Christopher H. Baker and Pamela M. Norris

Phys. Rev. B **91**, 180302 — Published 12 May 2015

DOI: [10.1103/PhysRevB.91.180302](https://doi.org/10.1103/PhysRevB.91.180302)

1 **The Effect of Long- and Short-Range Order on SiGe Alloy**
2 **Thermal Conductivity: Molecular Dynamics Simulation**

3 Christopher H. Baker* and Pamela M. Norris†

4 *Department of Mechanical and Aerospace Engineering,*

5 *University of Virginia, 122 Engineer's Way, Charlottesville, VA, 22904-4746*

6 (Dated: April 15, 2015)

7 **Abstract**

8 We report the role of long- and short-range order on the thermal conductivity and mode re-
9 laxation times of a model $\text{Si}_{0.5}\text{Ge}_{0.5}$ alloy using molecular dynamics simulation. All interactions
10 used the Stillinger-Weber potential and the Si and Ge atoms differed only by their mass. The
11 simulated alloys were generated using a Monte Carlo approach to decouple the short-range order
12 from the long-range order. The thermal conductivity is almost entirely determined by the alloy's
13 nearest-neighbor short-range order. Changes to the mode relaxation times between ~ 3 and ~ 6
14 THz upon short-range ordering, and the observed f^{-2} power law trend, suggests that short-range
15 ordering reduces the anharmonic scattering rate of low frequency modes. The trend of thermal
16 conductivity with short-range order may be transferred to real $\text{Si}_{0.5}\text{Ge}_{0.5}$ and other semiconductor
17 alloys to the extent that scattering from mass disorder dominates their thermal conductivities.

18 PACS numbers: 66.70.Df, 63.50.Gh, 61.66.Dk, 61.43.Bn

19 Altering the composition of $\text{Si}_{1-x}\text{Ge}_x$ and other alloys is one route for engineering their
 20 thermal conductivity, k .^{1,2} In addition to numerous experimental studies,³⁻⁶ there have been
 21 many recent computational studies of the thermal properties of SiGe using classical molecu-
 22 lar dynamics⁷⁻¹² and density functional theory.^{13,14} Studies have focused on the dependence
 23 of k on composition,^{7,14} grain size,¹⁰ nanoparticle inclusions,^{13,15} and nanowire boundary
 24 scattering,¹⁶ all in an effort to improve the thermoelectric figure of merit.^{17,18} Alloys possess
 25 two additional degrees of freedom for tuning k : the arrangement of the atoms on the lat-
 26 tice as characterized by the long-range¹⁹ and short-range²⁰ order parameters. In molecular
 27 dynamics studies of a Lennard-Jones alloy, Duda *et al.* showed that the long-range order
 28 can be used to tune k over an order of magnitude at low temperatures.^{21,22} Here, we take
 29 $\text{Si}_{0.5}\text{Ge}_{0.5}$ as a representative model for semiconductor alloys and we report the effect of
 30 long-range and short-range order on the thermal conductivity and normal mode relaxation
 31 times at 300 K using molecular dynamics simulation.

32 The Bragg-Williams long-range order parameter, \mathbb{L} , gives the probability that an atom
 33 occupies the correct lattice site with reference to the ordered structure, and the probability is
 34 duly normalized by the atom's concentration in the alloy.¹⁹ The Warren-Cowley short-range
 35 order parameters give the probability of an atom having the correct neighbor in a certain
 36 neighbor shell with reference to the ordered structure.²⁰ We define a set of short-range order
 37 parameters, \mathbb{S}_i , where i indexes the neighbor shells, as the square-root of the Warren-Cowley
 38 short-range order parameters so that $\lim_{i \rightarrow \infty} \mathbb{S}_i = \mathbb{L}$.^{20,23} Assuming an equimolar binary alloy
 39 for which each lattice site is eligible for a disordering substitution simplifies the expressions
 40 for \mathbb{L} and \mathbb{S}_i . Then, $\mathbb{L} \equiv |R-W|/N$, where R (W) is the number of atoms occupying the right
 41 (wrong) lattice site, and N is the total number of atoms.²³ Similarly, $\mathbb{S}_i \equiv \sqrt{|R_i - W_i|/N_i}$,
 42 where R_i , W_i , and N_i are the numbers of right, wrong, and total neighbor pairs in neighbor
 43 shell i , respectively.²³

44 Structures with varying \mathbb{L} and \mathbb{S}_1 can be generated by a Monte Carlo approach. For a
 45 binary alloy with the aforementioned simplifying assumptions, the seed structure is formed
 46 from the definition of \mathbb{L} and the compositional constraint. Beginning from a zincblende
 47 reference structure,²⁴ we randomly selected and exchanged n Si atoms and n Ge atoms,
 48 where $n = N(1 - \mathbb{L})/4$. At this point, $\mathbb{S}_i \approx \mathbb{L}$. Then, in each Monte Carlo step, we
 49 randomly selected atoms to swap that preserved the composition and \mathbb{L} , accepting swaps that
 50 brought \mathbb{S}_1 closer to the target value. No consideration has been given to the temperature

51 or configurational entropy of these structures—they are not in equilibrium. Control over \mathbb{L}
 52 and \mathbb{S}_i in actual $\text{Si}_{0.5}\text{Ge}_{0.5}$ requires a non-equilibrium growth process,^{25,26} which is likely the
 53 case for other semiconductor alloys too.

54 We used the Green-Kubo method^{27,28} at thermal equilibrium to measure k . The con-
 55 vergence time of the heat current auto-correlation function was determined by the *first*
 56 *avalanche* criterion²⁹ with an averaging window of 8.0 ps (8^3 and 12^3 conventional cell sam-
 57 ples) or 40.0 ps (18^3 , 28^3 , or 42^3 conventional cell samples) and a noise-to-signal cutoff of
 58 1000.³⁰

59 The relaxation times, $\tau(\nu)$, were calculated using the normal mode decomposition
 60 method²⁸ in the frequency domain.³¹ The atomic trajectories are projected onto the har-
 61 monic normal modes (calculated using GULP³²), then Fourier transformed and fit to a
 62 Lorentzian:

$$C \frac{\Gamma(\nu)/\pi}{(f - f_0(\nu))^2 + \Gamma^2(\nu)} = t_f^{-1} |\dot{Q}(\nu, f)|^2. \quad (1)$$

63 The fit yields $\tau = 1/(4\pi\Gamma)$ and the anharmonic linear frequency, f_0 , for each normal mode,
 64 ν . At thermal equilibrium, the coefficient C is guaranteed to be $\frac{1}{2}k_B T$ from the equipartition
 65 principle. The duration of data collection, t_f , ought to be much greater than the maximum
 66 $\tau(\nu)$ for the material.³³ \dot{Q} is the Fourier transform of the normal mode velocity coordinate,
 67 \dot{q} .³⁴ $\dot{Q} = \int_0^{t_f} \dot{q} \exp(-2\pi ift) dt$.³⁵ Due to the sharpness of the peak in $|\dot{Q}|^2$, we increased the
 68 weighting near the base by taking the decimal logarithm of each side of Eq. 1. Only points
 69 above 0.104 meV/THz ($1 \text{ amu} \cdot \text{\AA}^2 \cdot \text{ps}^{-1}$) were used in the fit. Because the global minimum
 70 of the root-mean-square of the residuals lay in a narrow well surrounded by local maxima,
 71 we found it necessary to do a grid search before regression, with 31 points linearly spaced
 72 between ± 0.1 THz of the peak frequency and 31 points logarithmically spaced between Γ of
 73 10^{-5} and 10^{-1} ps^{-1} .

74 All simulations were performed using LAMMPS³⁶ with a time step of 0.5 fs. The
 75 zincblende lattice constant was set to 5.43 \AA , and the Si and Ge atoms only differed in their
 76 masses: 28.09 and 72.64 amu respectively. The Stillinger-Weber potential³⁷ was used for all
 77 interactions since the effect of strain on k is small compared to that of mass disorder.⁷ The
 78 system was equilibrated at 300 K for 1 ns in a canonical ensemble enforced by a Nosé-Hoover
 79 thermostat^{38,39} with a coupling time of 2 ps. The system was then run for an additional
 80 1 ns in a microcanonical ensemble before data were collected for $36 \cdot 2^{17}$ time steps (2.36 ns),

FIG. 1. (color online) Short-range order parameters of the 8^3 unit cell SiGe structures. Each color represents a different long-range order and each line is the average of 10 independently generated samples.

FIG. 2. (color online) Thermal conductivities of the 8^3 unit cell SiGe structures. The thermal conductivity is constant within the uncertainty (2σ) along the rows, indicating that the short-range order is the dominant factor. Underlined data were also studied for size effects (Fig. 3).

81 printing the conduction term of the heat current every 10 time steps for calculating k ,⁴⁰ and
 82 printing atomic velocities every 36 time steps for calculating $\tau(\nu)$.

83 Ten independent samples of size 8^3 conventional cells were generated for each combination
 84 of \mathbb{L} and \mathbb{S}_1 in the range 0.0 to 0.9 for $\mathbb{S}_1 \geq \mathbb{L}$ and their thermal conductivities were
 85 calculated. The uncertainty in k is reported as twice the standard deviation of the ten
 86 calculated values. The relaxation times of 2000 normal modes were calculated for one
 87 sample of each set. These normal modes include all those below 3 THz (excluding the zero
 88 frequency modes) with the rest randomly distributed among the remaining modes. Size
 89 effects were explored for select pairs of \mathbb{L} and \mathbb{S}_1 by increasing the domain size to 12^3 , 18^3 ,
 90 28^3 , and 42^3 conventional cells and performing a linear extrapolation procedure.^{12,41,42}

91 While only \mathbb{S}_1 was used as a metric for the Monte Carlo generation, $\mathbb{S}(r)$, where r is the
 92 neighbor distance, systematically decreases towards \mathbb{L} (Fig. 1). One might characterize the
 93 approach of $\mathbb{S}(r)$ toward \mathbb{L} by a decay length scale, which would be less than 1.5 nm for each
 94 structure plotted in Fig. 1. The case $\mathbb{S}_1 > \mathbb{L}$ can be thought of as corresponding to an alloy
 95 composed of grains defined by anti-phase boundaries. Then, $\mathbb{S}(r)$ would scale with the mean
 96 grain size and \mathbb{L} would scale with the ratio of volumes occupied by phase and anti-phase
 97 grains. For structures with $\mathbb{L} = 0$, $\mathbb{S}(r)$ is substantially above zero at all neighbor distances
 98 (Fig. 1). This is a consequence of the small domain size and our choice to define \mathbb{S}_i using
 99 the square-root. The square-root amplifies the small deviations of $|R_i - W_i|/N_i$ from zero;
 100 the deviations of this ratio from the ideal value (defined with respect to \mathbb{L}) were about the
 101 same for all structures. The small domain size also inhibits the exact convergence of $\mathbb{S}(r)$
 102 to \mathbb{L} when $\mathbb{S}_1 \gg \mathbb{L}$. Nevertheless, the structures exhibit unique $\mathbb{S}(r)$ profiles.

103 To within the uncertainty, the thermal conductivity depends only on a structure's \mathbb{S}_1 , or
 104 possibly \mathbb{S}_i for small i (Fig. 2). Thus, \mathbb{L} affects k to the extent that it sets the lower limit for
 105 $\mathbb{S}(r)$. Consistent with the low temperature trend observed by Duda *et al.*,²² $\partial k / \partial \mathbb{S}_1$ increases

FIG. 3. (color online) Size effects on the thermal conductivity for select SiGe structures. Each filled symbol is the average of 10 samples. The arcs along the k axis indicate the 95% confidence interval of the intercept based on the 50 total samples for each $(\mathbb{L}, \mathbb{S}_1)$ pair. The intercepts are ordered by \mathbb{S}_1 and not \mathbb{L} , indicating that just as in Fig. 2, the bulk k is determined by \mathbb{S}_1 . Previous studies of the $\mathbb{L}=\mathbb{S}_1=0$ alloy are also plotted.

106 as \mathbb{S}_1 approaches one. We observe the same trend in k with respect to ordering because the
 107 structures investigated by Duda *et al.*,²² which were generated from the definition of \mathbb{L} ,
 108 always had $\mathbb{S}_i \approx \mathbb{L}$.

109 A phonon is insensitive to material heterogeneities with length scales much less than
 110 the phonon's wavelength. Instead, these phonons can be thought of as traveling through
 111 a material with effective, averaged properties, *e.g.* density and elastic moduli.² *Ab initio*
 112 calculations have shown that phonons with frequencies less than 2 THz carry 88% of the
 113 heat in SiGe.¹⁴ Making use of the dispersion calculated for an empirical model of SiGe,¹¹
 114 this translates to a phonon wavelength greater than ~ 3.0 nm (longitudinal) or ~ 1.8 nm
 115 (transverse) in our systems. These wavelengths are greater than the $\mathbb{S}(r)$ decay lengths of
 116 about 1.5 nm or less (Fig. 1), which would suggest a reduced dependence of k on \mathbb{S}_1 as the
 117 system size increases, introducing more long wavelength modes. Yet Fig. 3 shows that the
 118 strong dependence of k on \mathbb{S}_1 persists out to the bulk limit.

119 To explore the dependence of k on \mathbb{S}_1 further, Fig. 4 shows the normal mode relaxation
 120 times. Figure 4a compares our results for the completely disordered structure to previous
 121 molecular dynamics simulations using normal mode decomposition.^{9,11,12} Though each work
 122 investigated $\text{Si}_{0.5}\text{Ge}_{0.5}$ thermal conductivity at 300 K, slightly different simulation and fitting
 123 procedures were used. Our relaxation times agree with those of Hori *et al.*¹¹ The agreement
 124 with He *et al.*⁹ is also good, especially considering their use of a Tersoff potential⁴⁴ instead
 125 of the Stillinger-Weber potential. The relaxation times of Larkin and McGaughey¹² are
 126 significantly shorter than the others, although a similar trend is shown. The disagreement
 127 may be due to their use of the virtual-crystal modes for the normal mode decomposition.⁴⁵

128 Figures 4b,c and Fig. 4d show the mode relaxation times for two paths between the
 129 ordering extrema: $(\mathbb{L}, \mathbb{S}_1) = (0.0, 0.0) \rightarrow (0.9, 0.9)$. That Figs. 4c and 4d are so similar, and
 130 Fig. 4b shows no significant change in $\tau(\nu)$ with \mathbb{L} , supports the conclusion of Fig. 2: that
 131 \mathbb{S}_1 accounts for the entire change in k upon ordering.

132 The relaxation times below 10 THz are roughly fit by an f^{-2} power law (Figs. 4b-d).

FIG. 4. (color online) Mode relaxation times for slices through \mathbb{L} - \mathbb{S}_1 parameter space. (a) Comparison of our fully disordered SiGe structure to previous results. (b) Constant \mathbb{S}_1 slice. The majority of modes are unaffected by \mathbb{L} . Note the change in ordinate scale. (c) Constant \mathbb{L} slice. All modes are sensitive to \mathbb{S}_1 . (d) $\mathbb{L}=\mathbb{S}_1$ slice. The relaxation times are nearly identical to those of (c), in agreement with the thermal conductivity trends of Figs. 2 and 3.

133 The fitted exponents fell within -2 ± 0.15 for each plotted $(\mathbb{L}, \mathbb{S}_1)$ pair. The relaxation
 134 times below ~ 1.5 THz have a greater variance for two reasons. The total simulation time
 135 (4.36 ns) was comparable to the fitted relaxation time, so these modes are non-thermalized,
 136 invalidating the assumption of equipartition for those modes. The relaxation times are also
 137 comparable to the period of data collection, reducing the accuracy of the fit. It is likely
 138 that the power law trend in this regime continues as f^{-2} but with a reduced variance,^{2,14}
 139 although this cannot be verified by the present simulations.

140 Figures 4c and 4d also show a change in the character of the relaxation times, especially
 141 in the range of 3 to 6 THz. The curve is smooth for $\mathbb{S}_1=0$. But as \mathbb{S}_1 increases, peaks and
 142 valleys form where the momentum and energy selection rules for phonon scattering become
 143 more and less restrictive. Furthermore, a bandgap forms at ~ 11 THz.

144 We therefore attribute the dependence of k on \mathbb{S}_1 (instead of \mathbb{L}) to the alteration of
 145 the phonon eigenvectors caused by short-range ordering. As \mathbb{S}_1 increases, the eigenvectors
 146 approach those of the zincblende crystal. While high frequency modes might significantly
 147 contribute to k in the limit $\mathbb{S}_1 \rightarrow 1$, most of the increase for the ordering range studied here
 148 is caused by a reduction in the anharmonic scattering of the low frequency modes. The
 149 reduction in anharmonic scattering may be due to fewer states that satisfy momentum
 150 and energy selection rules, a reduction in the scattering cross-section, or both mechanisms.
 151 The same trend of k with disorder was observed Garg *et al.*, who saw a reduction in k
 152 with greater disorder, when they went from a virtual crystal to an explicitly disordered
 153 supercell.¹⁴ They found that the change in k was due to altered mode relaxation times,
 154 caused by a modification of the mode eigenvectors.

155 The findings may be cautiously generalized to other simulated and real alloys provided
 156 the thermal conductivities of their disordered states arise primarily from the same mech-
 157 anisms as those found in the present model of $\text{Si}_{0.5}\text{Ge}_{0.5}$, namely the scattering of lattice
 158 vibrations by mass disorder. That k depends almost solely on \mathbb{S}_1 has implications for the
 159 characterization and theoretical modeling of such alloys. When examining an alloy with

160 the purpose of understanding its thermal conductivity or predicting it, a characterization
161 technique sensitive to the short-range order must be used, *e.g.* diffuse X-ray scattering.⁴⁶
162 Similarly, future efforts to theoretically model thermal transport in ordered alloys should
163 focus on the short-range order or its effect on anharmonic phonon scattering.

164 In summary, we performed molecular dynamics simulations of a $\text{Si}_{0.5}\text{Ge}_{0.5}$ alloy, repre-
165 senting a model semiconductor alloy, and calculated the thermal conductivity as it depends
166 on the long- and short-range ordering. We found that the bulk thermal conductivity depends
167 almost wholly on the short-range order of the alloy for a fixed composition. Relaxation time
168 calculations support this dependence. Changes in the character of the mode relaxation times
169 upon ordering imply that the corresponding increase in thermal conductivity is caused by a
170 reduction in disorder-induced anharmonic phonon scattering.

171 ACKNOWLEDGMENTS

172 The authors thank T. Hori, J. Shiomi, Y. He, G. Galli, J. Larkin, and A. McGaughey
173 for sharing their relaxation time data. We are indebted to A. McGaughey and J. Larkin
174 for their comments and insights, and we thank L. Zhigilei for helpful discussion. This work
175 was supported by a grant from the National Science Foundation (CTS-1134301) and was
176 conducted with government support under contract FA9550-11-C-0028 and awarded by the
177 Department of Defense, Air Force Office of Scientific Research, National Defense Science and
178 Engineering Graduate (NDSEG) Fellowship, 32 CFR 168a. C. Baker gratefully acknowledges
179 the support from NDSEG and VSGC fellowships.

180 * chb2fd@virginia.edu

181 † pamela@virginia.edu

182 ¹ B. Abeles, D. S. Beers, G. D. Cody, and J. P. Dismukes, [Physical Review](#) **125**, 44 (1962).

183 ² B. Abeles, [Physical Review](#) **131**, 1906 (1963).

184 ³ S. T. Huxtable, A. R. Abramson, C.-L. Tien, A. Majumdar, C. LaBounty, X. Fan, G. Zeng,
185 J. E. Bowers, A. Shakouri, and E. T. Croke, [Applied Physics Letters](#) **80**, 1737 (2002).

186 ⁴ G. Joshi, H. Lee, Y. Lan, X. Wang, G. Zhu, D. Wang, R. W. Gould, D. C. Cuff, M. Y. Tang,
187 M. S. Dresselhaus, G. Chen, and Z. Ren, [Nano Letters](#) **8**, 4670 (2008).

188 ⁵ R. Cheaito, J. C. Duda, T. E. Beechem, K. Hattar, J. F. Ihlefeld, D. L. Medlin, M. A. Rodriguez,
189 M. J. Champion, E. S. Piekos, and P. E. Hopkins, *Physical Review Letters* **109**, 195901 (2012).

190 ⁶ R. B. Wilson and D. G. Cahill, *Nature Communications* **5**, 5075 (2014).

191 ⁷ A. Skye and P. K. Schelling, *Journal of Applied Physics* **103**, 113524 (2008).

192 ⁸ J. Chen, G. Zhang, and B. Li, *Applied Physics Letters* **95**, 073117 (2009).

193 ⁹ Y. He, I. Savić, D. Donadio, and G. Galli, *Physical Chemistry Chemical Physics* **14**, 16209
194 (2012).

195 ¹⁰ C. Abs da Cruz, N. A. Katcho, N. Mingo, and R. G. A. Veiga, *Journal of Applied Physics* **114**,
196 164310 (2013).

197 ¹¹ T. Hori, T. Shiga, and J. Shiomi, *Journal of Applied Physics* **113**, 203514 (2013).

198 ¹² J. M. Larkin and A. J. H. McGaughey, *Journal of Applied Physics* **114**, 023507 (2013).

199 ¹³ A. Kundu, N. Mingo, D. A. Broido, and D. A. Stewart, *Physical Review B* **84**, 125426 (2011).

200 ¹⁴ J. Garg, N. Bonini, B. Kozinsky, and N. Marzari, *Physical Review Letters* **106**, 045901 (2011).

201 ¹⁵ N. Mingo, D. Hauser, N. P. Kobayashi, M. Plissonnier, and A. Shakouri, *Nano Letters* **9**, 711
202 (2009).

203 ¹⁶ Z. Wang and N. Mingo, *Applied Physics Letters* **97**, 101903 (2010).

204 ¹⁷ A. J. Minnich, M. S. Dresselhaus, Z. F. Ren, and G. Chen, *Energy and Environmental Science*
205 **2**, 466 (2009).

206 ¹⁸ C. J. Vineis, A. Shakouri, A. Majumdar, and M. G. Kanatzidis, *Advanced Materials* **22**, 3970
207 (2010).

208 ¹⁹ W. L. Bragg and E. J. Williams, *Proceedings of the Royal Society of London A* **145**, 699 (1934).

209 ²⁰ J. M. Cowley, *Physical Review* **77**, 669 (1950).

210 ²¹ J. C. Duda, T. S. English, D. A. Jordan, P. M. Norris, and W. A. Soffa, *Journal of Physics:*
211 *Condensed Matter* **23**, 205401 (2011).

212 ²² J. C. Duda, T. S. English, D. A. Jordan, P. M. Norris, and W. A. Soffa, *Journal of Heat*
213 *Transfer* **134**, 014501 (2012).

214 ²³ H. Sato, in *Physical Chemistry: An Advanced Treatise*, Vol. 10, edited by W. Jost (Academic
215 Press, 1970) Chap. 10, p. 579.

216 ²⁴ The true ordered structure of $\text{Si}_{0.5}\text{Ge}_{0.5}$ consists of alternating bilayers of Si and Ge in the
217 [111] direction.⁴⁷ We took the zincblende structure as the reference since the usage of a single
218 potential for all interactions in the simulation gives all ordered structures equivalent potential

219 energy and many compound semiconductors do order into a zincblende structure, *e.g.* those of
220 Ref. 48.

221 ²⁵ P. C. Weakliem and E. A. Carter, *Physical Review B* **45**, 13458 (1992).

222 ²⁶ K. L. Whiteaker, I. K. Robinson, J. E. Van Nostrand, and D. G. Cahill, *Physical Review B*
223 **57**, 12410 (1998).

224 ²⁷ D. A. McQuarrie, *Statistical Mechanics* (University Science Books, 2000).

225 ²⁸ A. J. C. Ladd, B. Moran, and W. G. Hoover, *Physical Review B* **34**, 5058 (1986).

226 ²⁹ J. Chen, G. Zhang, and B. Li, *Physics Letters A* **374**, 2392 (2010).

227 ³⁰ In a minority of samples, the noise-to-signal never reached 1000. In these cases, the maximum
228 in the noise-to-signal determined the convergence time.

229 ³¹ J. M. Larkin, J. E. Turney, A. D. Massicotte, C. H. Amon, and A. J. H. McGaughey, *Journal*
230 *of Computational and Theoretical Nanoscience* **11**, 249 (2014).

231 ³² J. D. Gale and A. L. Rohl, *Molecular Simulation* **29**, 291 (2003).

232 ³³ Of course, t_f must be chosen before the maximal τ is known.

233 ³⁴ M. T. Dove, *Introduction to Lattice Dynamics* (Cambridge University Press, 1993).

234 ³⁵ Dropping the negative frequency component of $|\dot{Q}(f, \nu)|^2$ causes factors of two in Eq. 1 to cancel.
235 The linear, instead of angular, Fourier transform adds a factor of 2π to the expression for τ .
236 See Refs. 31 and 42.

237 ³⁶ S. Plimpton, *Journal of Computational Physics* **117**, 1 (1995).

238 ³⁷ F. H. Stillinger and T. A. Weber, *Physical Review B* **31**, 5262 (1985).

239 ³⁸ S. Nosé, *Journal of Chemical Physics* **81**, 511 (1984).

240 ³⁹ W. G. Hoover, *Physical Review A* **31**, 1695 (1985).

241 ⁴⁰ E. S. Landry, *Thermal transport by phonons across semiconductor interfaces, thin films, and*
242 *superlattices.*, Ph.D. thesis, Carnegie Mellon University (2009).

243 ⁴¹ J. Shiomi, K. Esfarjani, and G. Chen, *Physical Review B* **84**, 104302 (2011).

244 ⁴² A. J. H. McGaughey and J. M. Larkin, *Annual Review of Heat Transfer* **17**, 49 (2014).

245 ⁴³ J. M. Larkin, *Vibrational mode properties of disordered solids from high-performance atomistic*
246 *simulations and calculations*, Ph.D. thesis, Carnegie Mellon University (2013).

247 ⁴⁴ J. Tersoff, *Physical Review B* **39**, 5566 (1989).

248 ⁴⁵ The disagreement remains perplexing since their calculations of k using the virtual-crystal
249 normal mode relaxation times agree with the k calculated by the Green-Kubo method, as

250 plotted in Fig. 3 and Ref. 43. Furthermore, the virtual-crystal approximation with *ab initio*
251 force constants produced k values consistent with experiment at 300 K in Ref. 14.

252 ⁴⁶ B. E. Warren, *X-Ray Diffraction* (Addison-Wesley Publishing Company, Inc., 1969).

253 ⁴⁷ J. Z. Tischler, J. D. Budai, D. E. Jesson, G. Eres, P. Zschack, J.-M. Baribeau, and D. C.
254 Houghton, *Physical Review B* **51**, 10947 (1995).

255 ⁴⁸ I. Vurgaftman, J. R. Meyer, and L. R. Ram-Mohan, *Journal of Applied Physics* **89**, 5815 (2001).

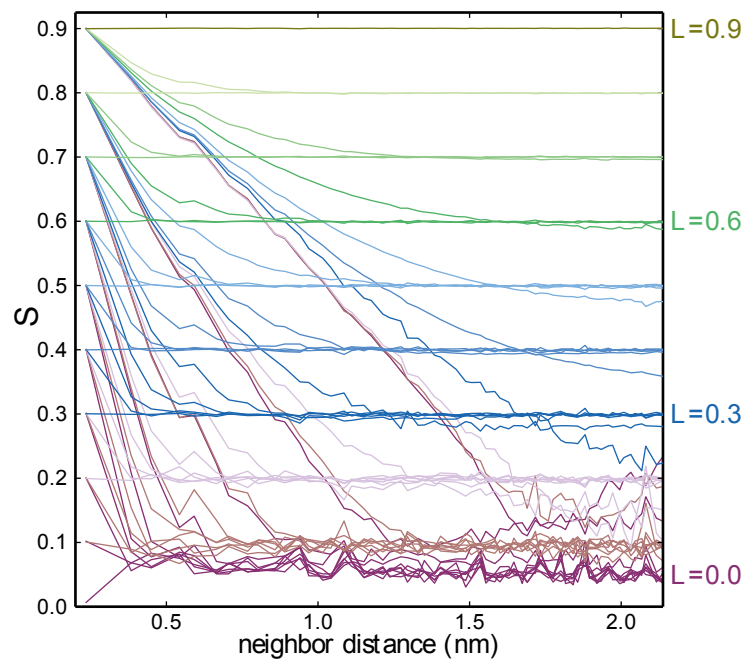


Figure 1

15Apr2015

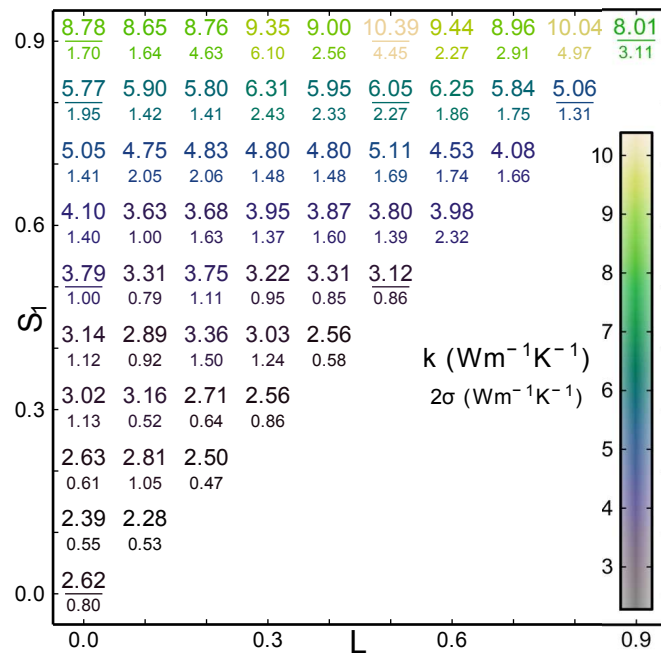


Figure 2

15Apr2015

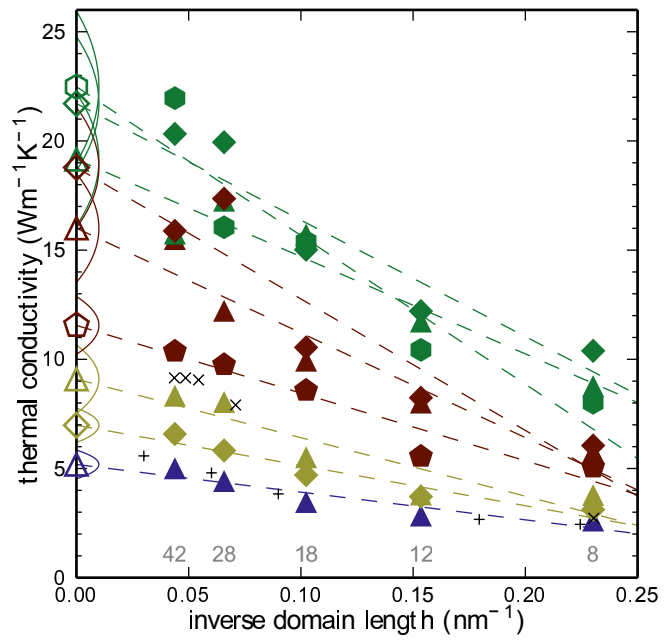


Figure 3

15Apr2015

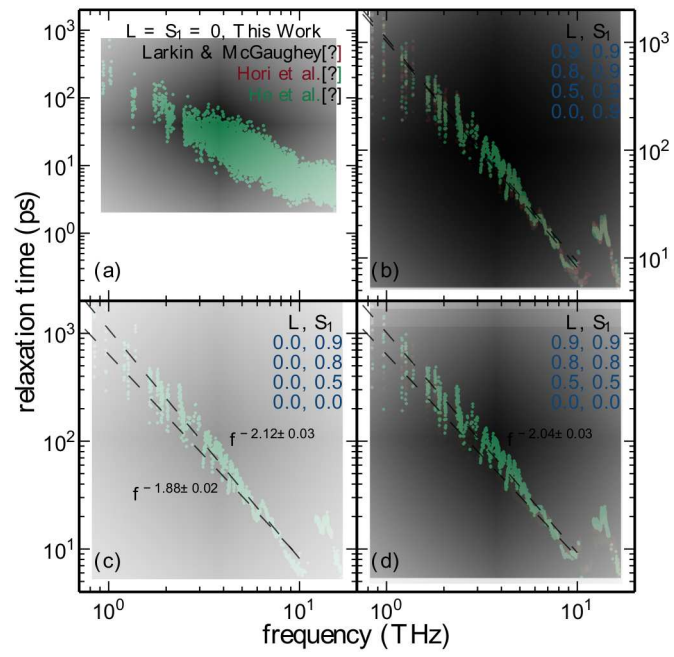


Figure 4

15Apr2015